HEFAT2011
8th International Conference on Heat Transfer, Fluid Mechanics and Thermodynamics
July 11-13, 2011
Pointe Aux Piments, Mauritius

INTERACTION BETWEEN THE JET AND WAKES AS A METHOD FOR PASSIVE CONTROL OF PLANE IMPINGING JETS

Trávníček Z.*, Tesar V. and Marsik F.
*Author for correspondence
Institute of Thermomechanics AS CR, v. v. i.
Dolejškova 5, 182 00 Prague,
Czech Republic,
E-mails: tr@it.cas.cz, tesar@it.cas.cz, marsik@it.cas.cz

ABSTRACT

A planar impinging air jet was experimentally investigated, with passive flow control as means of enhancement of impingement heat/mass transfer. The control was achieved by means of an array of small cylinders, fixed at the nozzle lips so as to bridge the nozzle exit gap. Experiments used mainly the naphthalene sublimation technique, with the resultant local mass transfer coefficient converted to prediction of the corresponding heat transfer by means of the heat/mass transfer analogy. Also measured were the local velocities. The experiment revealed the expected spatially periodical character of the flow field and heat/mass transfer distributions. To quantify the heat/mass transfer effects, three procedures are proposed. Compared with the standard planar impinging jet at the optimal nozzle-to-wall distance, the enhancement of the average heat/mass transfer was demonstrated to reach up to 8%.

INTRODUCTION

Fluid jets impinging on surfaces (IJs) are frequently used to achieve very intensive heat and mass transfer in many industrial applications such as cooling, heating and drying. The subject has been studied quite extensively, the majority of the references focusing on the continuous (steady) IJs case – see [1–9].

Although the continuous IJs can achieve a very high heat transfer rate, effects of unsteadiness can intensify the transport processes to even higher levels. For implementation of the unsteadiness, various methods of passive or active flow control can be used – see, e.g., Gad-el-Hak, [10]. The present study focuses on the passive flow control (sometimes called flow management rather than flow control – Fiedler and Fernholz, [11]). The advantage of the passive methods is that they require no auxiliary power – their action being based only on a purposeful modification of the nozzle geometry.

To generate a pulsatile flow character using a part of the power carried by the supplied fluid, various no-moving-part fluidic alternators can be used – see Tesař [12], and Seifert and Pastuer [13]. Well known are fluidic actuators generating jet flapping. They can be designed either with an external feedback loop (Viets [14], Raman *et al*. [15], Camci and Herr [16], Tesař *et al.* [17, 18]) or with an internal feedback action (Mi *et al.,* [19]). The latter may be particularly effective if they utilise the intrinsic instability of shear flows, leading to self-sustained oscillation (e.g. by Nathan *et al.* [20] and Page *et al.* [21]).

NOMENCLATURE

b	[m]	jet nozzle width, see Fig. 1
B_N		blockage ratio of the nozzle by the control cylinders, $B_N = nd/S$
CSN		slot nozzle equipped with an array of the cross cylinders, see Fig. 1
d	[m]	diameter of the control cylinder, see Fig. 1
D_n	[m^2/s]	mass diffusion coefficient of naphthalene vapor in air
h	[W/(m^{2}K)]	local heat transfer coefficient
h_m	[m/s]	local mass transfer coefficient
H	[m]	nozzle-to-wall spacing, see Fig. 1
IJ		impinging jet
k	[W/(m K)]	thermal conductivity of the working fluid (air)
n		number of the control cylinders, see Fig. 1
Nu		local Nusselt number, hb/k
Nu_0		stagnation Nusselt number
Pr		Prandtl number
Q	[m^3/s]	volume flow rate, measured by an orifice plate in the air supply
Re		Reynolds number of the plane jet, $U_N b/\nu$
Re_d		Reynolds number based of flow around the control cylinder, $U_N b/\nu$
S	[m]	test section span, see Fig. 1
Sc		Schmidt number for naphthalene vapor in air
Sh		local Sherwood number, $h_m b/ D_n$
Sh_0		stagnation Sherwood number
SN		baseline slot nozzle
t	[s]	time
T_w	[K]	wall temperature
U_N	[m/s]	area-averaged nozzle exit velocity, $U_N = Q/[bS(1-B_N)]$
u	[m/s]	magnitude of the local velocity
x, y, z	[m]	Cartesian coordinates, see Fig. 1
Δp	[Pa]	pressure drop on the nozzle
ρ	[kg/m^3]	density
ν	[m^2/s]	kinematic viscosity

The present paper focuses on the passive control method using vortex shedding from an obstacle inserted into the jet flow. In other words, the steady IJ is actuated by the periodic wake formed downstream from a bluff body in the jet. Several examples of this method can be found in literature. For an axisymmetric geometry, Herwig *et al*. [22] designed and experimentally tested an actuator producing three different variants of self-sustained periodical IJs. One of the arrangements (named the "Karman jet nozzle" [22]) used an axisymmetric nozzle with a ring obstacle inserted into the nozzle exit. Experiments verified the desirable heat transfer augmentation. A slight increase of the Nusselt number was at the stagnation point in the center, where the evaluated maximum increment effect was 10–15% – under the conditions of small nozzle-to wall distances ($H/D = 2$) and high Reynolds number ($Re = 22000$). The results were attributed to the unsteadiness involving additional turbulence generation in the nozzle exit. It has to be noted that the blockage of the nozzle exit produced a 13% increase of the remaining area-averaged nozzle exit velocity, when keeping constant volume supply flow rate. However the power increase necessary to overcome this blockage was not discussed in [22].

A plane jet with a small circular cylinder placed into the potential core of the jet was investigated by Hsiao *et al*. [23]. They made hot-wire anemometric measurements, having focused their attention on fluid dynamics of the jet-on-cylinder impingement, shear layer instability, and cylinder wake shedding. A self-sustained oscillation was generated by these interactions. The oscillation frequency (with nearly constant Strouhal number value 0.2) was concluded to be the result of the feedback mechanism and hydrodynamic instability.

Haneda *et al*. [24] proposed another method for generation of unsteadily impinging two-dimensional jets. In their layout an elastically supported bluff body was kept in self-sustained mechano-fluidic oscillation by the action of the cross flow. The body was a small circular cylinder positioned into the jet potential core. The cylinder could be supported either rigidly or flexibly. A rigidly suspended cylinder was found to deteriorates the heat transfer at the stagnation point location, while an enhancement occurred outside of the stagnation region. A flexible (spring-loaded) suspension of the cylinder caused an additional enhancement effect. The interaction between the vortex shedding from the cylinder and the supporting spring mechanism induced cross-stream oscillation of the cylinder, causing an effective actuation of the main jet flow. Under small nozzle-to wall distances $H/b = 3–5$, the stagnation Nusselt number was enhanced by about 20% compared to the reference IJ without the cylinder.

Another interesting effect, which is found to result from an insertion of an obstacle into IJ [25], is the *bistable and hysteretic behavior*. The bistability is defined as the lack of unicity of the relevant solutions of the governing equations, with existence of two stable steady states. The boundary conditions alone cannot determine uniquely which of these two states will take place. The character of the flow depends on the previous history of the changes of variables, and the relationship between the variables forms the so called hysteretic loop. The bistability of IJs occurs when the recirculation bubble of the separated flow downstream from the obstacle is comparable in size with the nozzle-to-wall spacing so that the separation bubble is influenced by the presence of the impinging wall. Two typical cases are the axisymmetric and the planar IJs. The former case is the annular IJ [26–35], the latter case is the dual-jet impingement generated by the two-slot nozzle [36–38].

In the *axisymmetric geometry* case, Maki and Yabe [26] experimentally investigated an annular IJ, and identified four flow regimes of the flow field. Three of these regimes were characterized as a recirculating unsteady flow. The other experimental study of the same authors [27], based on the hot-wire and naphthalene experiments and pressure distribution measurements, have revealed three flowfield patterns. However, no hysteresis was identified by Maki and Yabe [26, 27]. On the other hand, bistability and associated hysteretic character of an annular IJ was predicted by means of numerical simulations by Kokoshima *et al*. [28]. A hysteretic behavior of annular IJs known to be present in swirling jets and tornadoes were described, e.g., by Shtern and Hussain [29, 30], and Vanierschot and Van den Bulck [31].

Tesař and Trávníček in [32] discussed annular impinging jets by analyzing the results of numerical flowfield computations, in which five different flow regimes were identified at different wall-to-nozzle distances. Bistability of the demarcation boundary between two of these regimes was demonstrated. However, no hysteresis was identified in the flows with the used geometry.

Bistable annular IJs under an active flow control were studied by Peszyński [33] and Trávníček *et al*. [34]. The hysteretical behavior was identified. Unfortunately, in this case it was an unwanted effect because it complicated controllability of the flow. Therefore, passive flow control was used by which the hysteresis was completely suppressed [34].

Another variant of an annular impinging jet was investigated experimentally by means of mass transfer (naphthalene sublimation) and wall pressure measurements by Trávníček and Tesař in [35]. The existence of the bistable and hysteretic behavior was confirmed. While a flow pattern A was characterized by small size of the recirculation bubble of the separated flow immediately downstream from the nozzle, the other pattern B exhibited a large recirculation region of the separated flow, reaching up to the impingement wall.

For the *planar geometry*, the phenomena of bistability and hysteresis of IJs were investigated experimentally by Trávníček and Křížek [36]. They measured a two-dimensional IJ issuing from a two-slot nozzle, i.e. from a slot divided into two by a central inserted fixed obstacle. An advanced variant of this geometry was studied by Trávníček and Maršík [37], and the hysteretic behavior was identified at a relatively large range of the nozzle-to wall-distances $6.5b–10.0b$ (where b is the sum of two widths of both nozzle halves).

Akiyama *et al.* [38] investigated the flow field and heat transfer in another variant of the dual-jet impingement, incorporating a periodic injection-suction forcing at the nozzle lips. They chose for their tests a rather small nozzle-to-wall distance, $H/b = 2$, and therefore they could not find the hysteresis and bistability. Obviously, they focused on the

regime with the large recirculation area of the separated flow, reaching up to the impingement wall (the flow pattern B in terms of ref. [35]), and they concluded that the forcing increased the stagnation Nusselt number by about 10% compared to the unforced case [37].

EXPERIMENTAL SETUP AND METHODS

Figure 1 shows the schematic view of the configuration tested in the present study. Experiments were conducted with air as the working fluid. The air was supplied by blowers (driven by 2 kW electric motor with speed control) and passed through an orifice plate used for flow rate measurement, into the large settling chamber. This was shaped as a vertical cylinder of 1 m x 1 m diameter x length size. The air then passed through series of screens and the honeycomb before entering the test section through the investigated nozzle. Figure 1 shows the nozzle, having the exit width b = 10.0 mm while the length, equal to the width of the test chamber downstream, was S = 130 mm. This means the nozzle aspect ratio was S/b = 13.0. This simple baseline slot nozzle is referred to by the abbreviation SN.

In the nozzle version for the passive flow control, there were fixed at the nozzle lips an array of n = 6 control cylinders (of 2.0 mm diameter each) spanning the exit gap at equidistant spacings 20 mm – see Fig. 1. The blockage of the baseline SN caused by the presence of these control cylinders was $B_N = nd/S$ (= 9.2%). The nozzle equipped with this array of cylinders is referred to by the abbreviation CSN.

A plane impingement wall was inserted opposite to the nozzle exit. The wall was the top surface of naphthalene plate as described below. To ensure nominal two-dimensionality, the test chamber was bounded at the front and rear by the pair of identical Perspex endwalls, seen in Fig. 1. Because of this arrangement, the entrainment from the ambient atmosphere could occur only in the direction normal to the nozzle lips. The endwalls covered the region from x = –200 mm to x = +200 mm. Shown in Fig. 1 is also the used x, y, z coordinate system.

The mean nozzle velocity U_N was evaluated from the volume flow rate Q, measured by the above mentioned orifice plate, as $U_N = Q/[bS(1-B_N)]$. Obviously, the velocity of the baseline SN without blockage was $U_N = Q/bS$. The Reynolds number of the jet flow was defined as $Re = U_N b/\nu$, where ν is the kinematic viscosity of air. The Reynolds number based on the control cylinder is defined as $Re_d = U_N b/\nu$. The investigated nozzle-to-wall distance was mostly $H = 10.0b$. It should be noted that this is the optimal value of IJ for the baseline SN (Martin [4]). The range of the Reynolds numbers was Re = 13300–20400 and Re_d = 2700–4100.

Experiments were performed inside the test chamber: width 1.3 m x depth 0.8 m x height 1.8 m. The main part of the present experimental investigations was made by the naphthalene sublimation method. This is the reason why the test chamber space was well ventilated to outside atmosphere. Measurements of the local velocity were performed by means of the three-hole cylindrical probe of 2.3 mm diameter, connected to an electronic manometer. Moreover, the pressure

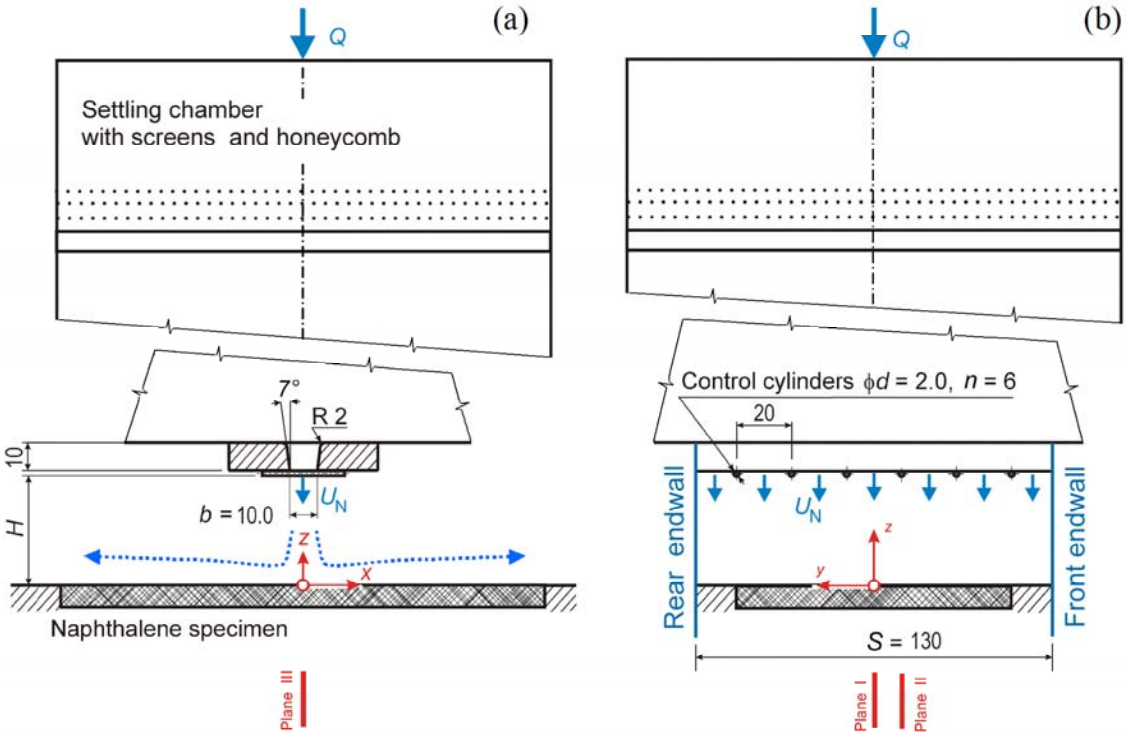

Figure 1 Impinging jet configuration tested in this study, sizes are in mm; the settling chamber is not scale drawing; (a) front view, (b) side view

drop Δp on the SN and CSN was measured by means of another electronic manometer.

Distribution of the local mass transfer coefficient was measured using the naphthalene sublimation method. The test specimen, produced by naphthalene casting, was of 100 mm x 420 mm active surface region. Following the descriptions by Trávníček *et al*. [34] and Goldstein and Cho [39], the mass transfer coefficient is evaluated as

$$h_m = \rho_n R_n T_w \Delta y / (p_{sat} \Delta t), \qquad (1)$$

where ρ_n is the density of solid naphthalene, R_n is the gas constant for naphthalene vapor, T_w is the surface temperature, Δy is the net local sublimation depth, p_{sat} is the saturated vapor pressure of naphthalene at T_w [38], and Δt is the run duration.

The non-dimensional parameter used to characterize the mass transfer coefficient is the Sherwood number, $Sh = h_m b/D_n$, where b is the nozzle exit width and D_n is the mass diffusion coefficient of naphthalene vapor in air, calculated for measured temperature and pressure conditions [39]. Uncertainty analysis was performed according to Kline and McClintock's [40] method for a single sample experiment. The uncertainty of the mass transfer coefficient and the Sherwood number was within 6% and 9%. A more detailed description of the experimental method and its uncertainties is available in Trávníček *et al*. [34].

RESULTS AND DISCUSSION

The first experimental investigations studied the properties of the baseline SN nozzle. Measurements of the velocity profiles in the exit of this nozzle have shown satisfactory uniformity. Presented in Fig. 2 is the time-mean velocity profile in the test section, measured by traversing the probe in the central plane III (as it is shown in Fig. 1). The otherwise practically constant velocity decreases – of course – in the boundary layers that developed on the Perspex endwalls.

The analogous velocity profiles obtained with CSN, presented also in Fig. 2, show the spatially periodic character of the velocity magnitude: the time-mean velocity is seen to decrease in the wakes downstream from each of the control cylinders (planes II). The flowfield in these wakes is of oscillatory character – in the turbulence there is a significant coherent component resulting from the vortex shedding from the cylinders. The Reynolds numbers and cylinder-to-wall distance are Re = 18400–19100, Re_d = 3800 and H/b = 10, i.e. H/d = 50.

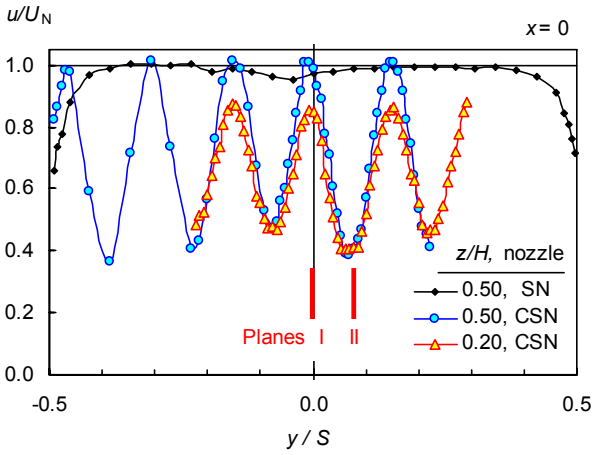

Figure 2 Streamwise velocity component for a measurement along plane III at H/b = 10, and Re = 18400 (SN) and 19100 (CSN)

The local time-mean mass transfer coefficient was evaluated by means of naphthalene sublimation experiments using Eq. (1). Following the heat/mass transfer analogy [4, 5, 39], the result was converted into the corresponding Nusselt number ratio $Nu/Pr^n = Sh/Sc^n$ to predict the heat transfer distribution. The exponent was taken to be n = 0.4 in this study, in agreement with [4, 5, 39].

Figure 3 presents an example of the transfer coefficient measurements with the baseline SN at the nozzle-to-wall spacing H/b = 4 and 10. The symmetry of the profiles indicates a very good symmetry of the whole flow field. The highest transfer rate values occur at the central stagnation line. For the larger H/b = 10, $Nu(x)$ is seen in Fig. 3 to decrease in a monotonous, "bell-shaped" manner with the distance from this line. For the smaller H/b = 4, the so-called "secondary peaks" of the heat transfer distribution occur distinctly at x/b = 7–8. These results agree well with the data in literature [1–7].

To verify the present method and setup, the maximum heat transfer rate at the central stagnation line is compared with three representative correlation equations as they were proposed by Korger and Křížek [1], Gardon and Akfirat [2], and Kumada and Mabuchi [3]. For the comparison purposes, the experimental correlation of [1] was modified (taking into account different Reynolds number definition and slightly different material properties) into the following form

$$Sh_0 = 0.679\,(H/b)^{-0.66}\,Re^{0.66}\,Sc^{1/3}, \qquad (2)$$

which is valid in the range of H/b = 8.5–40 and Re = 6400–38000.

Table 1 compares the three above mentioned predictions of the stagnation heat/mass transfer with the present experimental result from Fig. 3 at H/b = 10 (the optimum for IJ from SN [4])

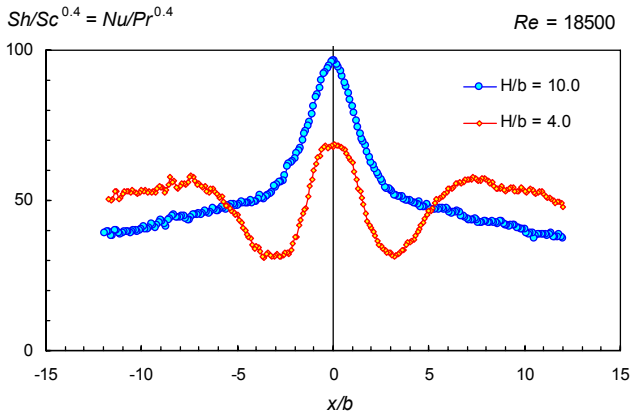

Figure 3 Local heat/mass transfer distribution, baseline SN

and $Re = 18500$. The differences between the values $Sh_0/Sc^n = Nu_0/Pr^n$ of the correlation Eqs. (2), [2], and [3] and the present experiment are –5%, +2%, and +8%, respectively. This reasonable agreement indicates acceptability of the present method. Another verification based on the average heat/mass transfer is presented at the end of this article as Fig. (8).

Table 1 Comparison of the stagnation heat/mass transfer for $H/b = 10$ and $Re = 18500$

	Experimental method	$Sh_0/Sc^{0.4} = Nu_0/Pr^{0.4}$
Eq. (2), modified from Korger & Křížek [1]	naphthalene sublimation	92.1
Gardon & Akfirat [2]	Gardon gage (heat-flow transducer)	98.4
Kumada & Mabuchi [3]	naphthalene sublimation	104.6
Present experiment	**naphthalene sublimation**	**96.7**

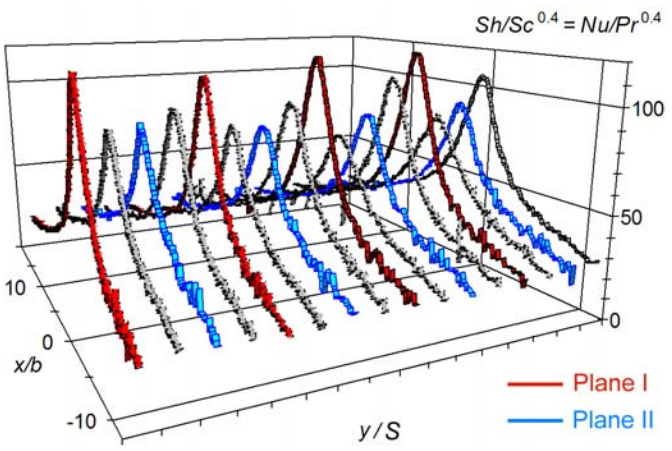

Figure 4 Local heat/mass transfer distribution, investigated CSN, $H/b = 10$ and $Re = 20000$

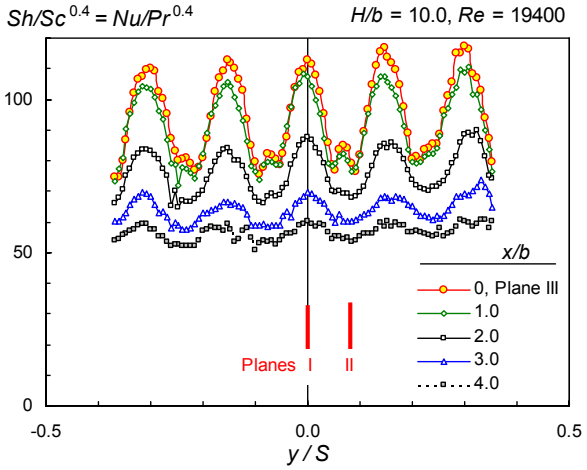

Figure 5 Distribution of heat/mass transfer along the stagnation line (plane III) and parallel planes; investigated CSN at $H/b = 10.0$ and $Re = 19400$

The next Fig. 4 shows the local heat/mass transfer distributions on the impingement wall obtained with the investigated CSN at $H/b = 10.0$ and $Re = 20000$. The results are shown in the shape of the three-dimensional projection of the ratio $Nu/Pr^n = Sh/Sc^n$ above the impingement wall. The highest heat/mass transfer rate occurs along the stagnation line $x = 0$. Moreover, the spanwise wavy character well corresponds to the spatially periodic character of the flow field (cf. Fig. 2) in this direction. The velocity decrease in the wake downstream from the control cylinder (plane II) qualitatively agrees with the decrease of the local heat/mass transfer there. To show this result in more detail, Fig. 5 presents the distribution of heat/mass transfer rate along the stagnation line (plane III) and along the parallel planes. This result confirms the finding from Fig. 4, i.e. the spatially periodic character in the spanwise direction (i.e. the direction of the nozzle slit length). Moreover, a non-monotonous character of the heat/mass transfer distribution in the cylinder wake along the plane II is revealed: instead of the simple local minimum at the plane II (as could be expected from a rough traversing grid in Fig. 4), the much finer traversing grid of Fig. 5 reveals a small local maximum there. It may indicate a complex character of flow around this place. It is possible to speculate that a saddle point and a reverse stagnation point (in terms of Maki and Yabe [26]) may occur near the plane II on the impingement wall. However, details of the surface streamline topology lay outside of the scope of the present study.

The impingement heat transfer obtained with CSN may be compared with the results of the baseline SN. For this reason, three cases of the baseline SN are considered, related to three comparison procedures A, B, and C. The comparisons are performed at:

A, identical mass flux, $Q\rho$

B, identical pumping power as the product of the volume flux and pressure drop, $Q\Delta p$

C, identical area-averaged nozzle exit velocity U_N

Note that the comparison procedure A is highly popular, see e.g. Herwig *et al.* [22] and Huang and El-Genk [41]. However, the present authors prefer the variant B, because it avoids too optimistic conclusions. The passive flow control devices in general increase the pressure drop, and keeping the constant mass flux (according to A) increases the pumping power. In other words, the passive flow control can yield seemingly enhancement effects, but the real effect is clouded by the penalty of the pumping power increase.

To advocate our approach and to elucidate the differences in the procedures A, B, and C, the following quantifications are made with all three procedures. The evaluation is performed for $Re = 20000$. For this reason, the original data from Fig. 5 for $Re = 19400$ were slightly corrected, based on the proportionality $Nu_0 \sim Re^{0.66}$ of Eq. (2), which results in the correction coefficient $(20000/19400)^{0.66} = 1.020$. Similar correction was applied to the present SN data ($Re = 18500$, Fig. 3) with three correction coefficients being 1.000, 1.037, and 1.066 for A, B and C procedure, respectively. The resultant comparison of the heat/mass transfer along the stagnation line (plane III) is shown in Fig. 6. The distribution relating to CSN varies in the oscillatory manner along the level relating to the

baseline SN. However, no significant enhancement effect is indicated there. This comparison is summarized in Table 2. The comparison procedures A, B, C yield a negligibly small average gain in the stagnation line: +3%, –1%, and –4%, respectively.

Table 2 Comparison of heat/mass transfer at the stagnation line for the investigated CSN and baseline SN

Nozzle	Comparison Procedure	*Re*	*P* [W]	$Sh_0/Sc^{0.4}$ $=Nu_0/Pr^{0.4}$	Gain of CSN %
CSN	-	20000	24.6	99	-
SN	A	18500	20.8	97	3
SN	B	19600	24.6	100	-1
SN	C	20400	27.8	103	-4

Another presentation of the data from Fig. 4 is shown in Fig. 7. The results were corrected again for $Re = 20000$, and transformed into the three curves: the planes I and II represent an average of measurements along four of these planes, i.e. between the cylinders and in their wakes, respectively. The curve labeled AV in Fig. 7 represents the result of averaging across the entire span of the test section. For comparison purposes, Fig. 7 shows the heat/mass transfer distribution of the baseline SN from Fig. 3 (corrected into $Re = 19600$, which corresponds to the procedure B according to Table 2). Fig. 7 shows a slight enhancement effect, about 13% at $x/b = 2.6$–2.8.

To quantify the integral heat/mass transfer, the local distribution is integrated into the average one as

$$Nu_L = (1/L) \int_{-L/2}^{L/2} Nu(x)\, dx \,. \qquad (3)$$

Figure 8 compares the average heat/mass transfer of CSN and SN showing that the maximum gain is 8% at $x/b = 3.1$–3.6, as is illustrated by the two arrows. Note that the most optimistic comparison by the procedure A gives an even higher value of 12%.

It is worthy to note here that the comparison is made purposely at the nozzle-to-wall distance $H/b = 10$, which is the optimum value for the baseline SN – see Martin [4]. It is possible to evaluate whether the present passive control method can yield even higher heat transfer rate values at distances different from what is the optimal arrangement for the baseline SN.

To verify once more the present experimental method and setup, the comparison in Fig. 8 is completed by addition of the reference correlation equation by Martin [4]. The differences are satisfactorily small, with the maximum 9% at the lower border of the validity range of [4], $x/b = 4$. For higher x/b the differences are smaller, though not negligible.

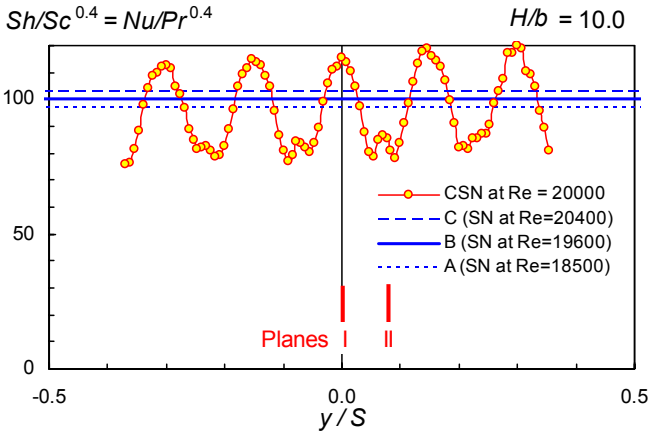

Figure 6 Comparison of investigated CSN and baseline SN, distribution of heat/mass transfer along the stagnation line (plane III) for $H/b = 10.0$

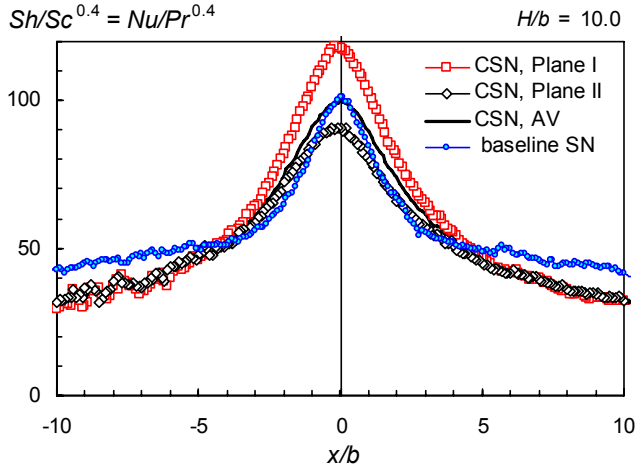

Figure 7 Local heat/mass transfer distribution. Comparison of investigated CSN at Re=20000 and baseline SN at $Re = 18500$ (see Table 2, A- procedure)

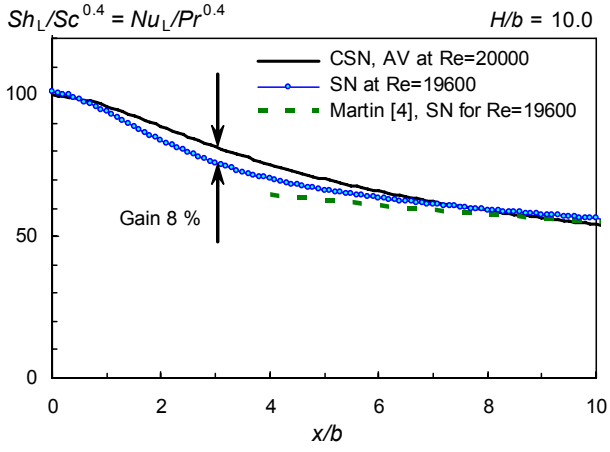

Figure 8 Average heat/mass transfer, comparison of investigated CSN and baseline SN

CONCLUSIONS

The planar impinging air jet was experimentally investigated. A passive flow control was applied in a form of an array of control cylinders inserted into the nozzle exit across the nozzle slit. The aim of the geometry modification was an enhancement of the impingement heat/mass transfer rate.

The present experiments demonstrate that the control cylinders generate an array of wakes. This causes a spatially periodic character of the flow field. Similarly, the impingement heat/mass transfer distribution is spatially periodic as well. To quantify the resultant enhancement effects, three procedures are proposed and discussed. They are based on the (A) identical mass flux, (B) identical pumping power (product of the volume flux and pressure drop), and (C) identical area-averaged nozzle exit velocity. The authors prefer B variant; the reasoning for this choice is presented.

The data show that the maximum enhancement of the average heat/mass transfer can reach the value 8% compared with the optimal baseline plane impinging jet at the identical pumping power.

Acknowledgement
We gratefully acknowledge the support of the Grant Agency AS CR (project No. IAA 200760801), GA CR – Czech Science Foundation (No. 101/09/1959), and Ministry of Education, Youth and Sports of the Czech Republic (No. 1M06031).

REFERENCES

[1] Korger M., and Křížek F., Mass-transfer coefficient in impingement flow slotted nozzles. International Journal of Heat and Mass Transfer, Vol. 9, No. 5, 1966, pp. 337–344.

[2] Gardon R., and Akfirat J.C., Heat transfer characteristics of impinging two-dimensional air jets. Trans. ASME, Journal of Heat Transfer, Vol. 88, No. 1, 1966, pp. 101–108.

[3] Kumada M., and Mabuchi, I., Studies on the heat transfer of impinging jet: 1st report, mass transfer of two-dimensional jet of air impinging normally on a flat plate. *Bulletin of the JSME*, Vol. 13, No.55, 1970, pp. 75–85.

[4] Martin H., Heat and mass transfer between impinging gas jets and solid surfaces, *Advances in Heat Transfer*, Vol. 13, 1977, pp. 1–60.

[5] Dyban E.P., and Mazur A.I., Convection Heat Transfer In Impinging Jets, (Konvektivnyj Teploobmen Pri Strujnom Obtekanii Tel), 1st Ed., Naukova Dumka, 1982, Kiev, (in Russian).

[6] Jambunathan K., Lai E., Moss M.A., and Button B.L., A review of heat transfer data for single circular jet impingement, *International Journal of Heat and Fluid*, Vol. 13, No. 2, 1992, pp. 106–115.

[7] Garimella, S.V., Heat transfer and flow fields in confined jet impingement, *Annual Review of Heat Transfer*, Vol. 11, 2000, pp. 413–494.

[8] Downs S.J., and James E.H., Jet impingement heat transfer – a literature survey. In: *Proceedings of the National Heat Transfer Conference*, ASME, Pennsylvania, USA, 1987, 87-HT-35.

[9] Webb B.W., Ma C.-F., Single-phase liquid jet impingement heat transfer, *Advances in Heat Transfer*, Vol. 26, 1995, pp. 105–107.

[10] Gad-el-Hak M., Modern developments in flow control, *Applied Mechanics Reviews*, Vol. 49, 1996, pp. 365–379.

[11] Fiedler H.E., and Fernholz H.H., On management and control of turbulent shear flows, *Progress in Aerospace Sciences*, Vol. 27, 1990, pp. 305–387.

[12] Tesař V., Pressure-Driven Microfluidics. Artech House Boston, Massachusetts, USA, 2007.

[13] Seifert A., and Pastuer S., Method and mechanism for producing suction and periodic excitation flow. US Patent No. 7,055,541 B2, 2006.

[14] Viets H., Flip-flop jet nozzle, *AIAA Journal* , Vol. 13, No. 10, 1975, pp. 1375–1379.

[15] Raman G., Rice E.J., and Cornelius D.M., Evaluation of flip-flop jet nozzles for use as practical excitation devices. *Trans. ASME, Journal of Fluids Engineering,* Vol. 116, 1994, pp. 508–515.

[16] Camci, C. , and Herr F., Forced convection heat transfer enhancement using a self-oscillating impinging planar jet. *Trans. ASME, Journal of Heat Transfer*, Vol. 124, 2002, pp. 770–782.

[17] Tesař V., Hung C-H., and Zimmerman W.B., No-moving-part hybrid-synthetic jet actuator, *Sensors and Actuators A* 125 (2) (2006) 159–169.

[18] Tesař V., Trávníček Z., Kordík J., and Randa Z., Experimental investigation of a fluidic actuator generating hybrid-synthetic jets*, Sensor and Actuators A*, Vol. 138, No. 1, 2007, pp. 213–220.

[19] Mi J., Nathan G.J., and Luxton R.E., Mixing characteristics of a flapping jet from a self-exciting nozzle, *Flow, Turbulence and Combustion*, vol. 67, 2001, pp. 1–23.

[20] Nathan G.J., Hill S.J., and Luxton R.E., An axisymmetric "fluidic" nozzle to generate jet precession. *Journal of Fluid Mechanics*, Vol. 370, 1998, 347–380.

[21] Page R.H., Chinnock P.S., and Seyed-Yagoobi J., Self-oscillation enhancement of impingement jet heat transfer, *AIAA Journal of Thermophysics and Heat Transfer*, Vol. 10, No. 2, 1996, pp. 380–382.

[22] Herwig H., Mocikat H., Gürtler T., and Göppert S., Heat transfer due to unsteadily impinging jets, *International Journal of Thermal Sciences,* Vol. 43, No. 8, 2004, pp. 733–741.

[23] Hsiao F.-B., Chou Y.-W., and Huang J.-M., The study of self-sustained oscillating plane jet flow impinging upon a small cylinder. *Experiments in Fluids*, Vol. 27, 1999, pp. 392–399.

[24] Haneda Y., Tsuchiya Y., Nakabe K., and Suzuki K., Enhancement of impinging jet heat transfer by making use of mechano-fluid interactive flow oscillation. *International Journal of Heat and Fluid Flow*, Vol. 19, No. 2, 1998, pp. 115–124.

[25] Tesař V., and Trávníček Z., Excitational metamorphosis of surface flowfield under an impinging annular jet**,** *Chemical Engineering Journal*, Vol. 144, No. 2, 2008, pp. 312–316.

[26] Maki H., and Yabe A., Unsteady characteristics of the annular impinging jet flow field and reverse stagnation

point heat transfer. *Proceedings of the National Heat Transfer Conference Heat Transfer in Convective Flows*, Philadelphia, PA, 1989, HTD, Vol. 107, 163–168.

[27] Maki H., and Yabe A., Heat transfer by the annular impinging jet, *Experimental Heat Transfer*, Vol. 2, 1989, pp. 1–12.

[28] Kokoshima Y., Shimizu A., and Murao T., Numerical Analysis of Annular Turbulent Jet Impinging on a Flat Plate. *Proceedings of the 3rd Triennial Int. Symp. Fluid Control, Measurement, And Visualization, FLUCOME'91*, ASME, San Francisco, USA, 1991, pp. 205–210.

[29] Shtern V., and Hussain F., Hysteresis in a swirling jet as a model tornado, *Physics of Fluids A*, Vol. 5, No. 9, 1993, pp. 2183–2195.

[30] Shtern V., and Hussain F., Hysteresis in swirling jets, *Journal of Fluid Mechanics*, Vol. 309, 1996, pp. 1–44.

[31] Vanierschot M., and Van Den Bulck E., Hysteresis in flow patterns in annular swirling jets, *Experimental Thermal and Fluid Science*, Vol 31, No. 6, 2007, pp. 513–524.

[32] Tesař V., and Trávníček Z., Review: Increasing heat and/or mass transfer rates in impinging jets, *Journal of Visualization*, Vol. 8, No. 2, 2005, pp. 91–98.

[33] Peszyński K., Flow control by axisymmetric fluidic device with radial switching. *Proceedings of the Engineering Mechanics '98, Svratka, Czech Republic,* 1998, pp. 583–588.

[34] Trávníček Z., Peszyński K., Hošek J., and Wawrzyniak S., Aerodynamic and mass transfer characteristics of an annular bistable impinging jet with a fluidic flip-flop control, *International Journal of Heat and Mass Transfer*, Vol. 46, No. 7, 2003, pp. 1265-1278.

[35] Trávníček Z., and Tesař V., Hysteretic behavior of annular impinging jets. *Proceedings of the 5th European Thermal-Sciences Conference*, Eindhoven, May 18–22, 2008, No. JET 6.

[36] Trávníček Z., and Křížek F., Impaktströmung und die Zusammengesetzte Schlitzdüse (Impinging jet and combined slot nozzle), *Heat and Mass Transfer*, Vol. 35, No. 5, 1999, pp. 351–356, (in German).

[37] Trávníček Z., and Maršík F., Flow visualization and mass transfer with a bistable two-slot impinging jet, *Journal of Visualization*, Vol. 6, No. 4, 2003, pp. 337–441.

[38] Akiyama T., Yamamoto K., Squires K.D., Hishida K., Simulation and measurement of flow and heat transfer in two planar impinging jets, *International Journal of Heat and Fluid Flow*, Vol. 26, 2005, pp. 244–255.

[39] Goldstein R.J., and Cho H.H., A review of mass transfer measurements using naphthalene sublimation, *Experimental Thermal and Fluid Science*, Vol. 10, 1995, pp. 416–434.

[40] Kline S.J., and McClintock F.A., Describing uncertainties in single-sample experiments. *Mechanical Engineering*, Vol. 75, 1953, pp. 3–8.

[41] Huang L., El-Genk M.S., Heat transfer and flow visualization experiments of swirling, multi-channel, and conventional impinging jets. *International Journal of Heat and Mass Transfer*, Vol. 41, No. 3, 1998, pp. 583–600.